Journal of Colloid and Interface Science **227,** 191–205 (2000)
doi:10.1006/jcis.2000.6877, available online at http://www.idealibrary.com on IDEAL®

A Mathematical Model for Crater Defect Formation in a Drying Paint Layer

P. L. Evans, L. W. Schwartz,[1] and R. V. Roy

Department of Mechanical Engineering, University of Delaware, Newark, Delaware 19716

Received December 8, 1999; accepted March 23, 2000

Certain deep indentations observed in dry coatings are referred to as "craters." They are believed to arise from gradients in the coating surface tension. A mathematical model of surface-tension-gradient-driven flow, using the lubrication approximation for thin layers, is developed to study the formation of craters. The paint is modeled as consisting of an evaporating "solvent" part and a nonvolatile "resin" part. Surface tension gradients on the coating surface arise due to a nonuniform distribution of surfactant. Axisymmetric numerical simulations using the model are performed to explore two candidate crater production mechanisms: an initial release of concentrated surfactant and a steady surfactant source. The effects of changes in various properties, such as the paint drying rate, the surfactant diffusivity, and the viscosity increase during drying, are examined. The model produces craters with large diameters, pronounced rims, and central peaks, similar to those seen in practice. Drying rate has a large influence on crater diameter and depth, by limiting flow due to surface tension gradients within a given time. Reduction of the paint viscosity increase during drying causes increased flow rates, leading to larger craters. A preexisting layer of surfactant on the paint surface sharply reduces the extent of cratering. Surfactant diffusion also tends to reduce the severity of cratering by alleviating surface tension gradients. In some cases, a simplified form of the drying model may be used to quickly approximate the results of the full model. The model provides useful insights into the craters seen in industrial coating applications.

Key Words: **craters; coatings; surface tension gradients; numerical simulation.**

1. INTRODUCTION

Production of a smooth, defect-free finish is the goal of many coating processes. Cratering is one of several defects which can occur during the drying of a painted surface, in which a circular depression appears in the dried film (1, 2). Often these craters have a raised outer rim; they may also have a central peak. They apparently occur while the painted layer is still wet enough to flow. Cratering during production can cause considerable costs to be incurred. For instance, even a few dozen craters forming during coating of a car body can halt production (3). Such craters may arise as the result of overspray, in which paint droplets are carried onto a still-wet coating on a previously painted car on a production line (4). Furthermore, eliminating coating defects has proved difficult, and fixing one problem can lead to the appearance of others (2).

Hahn and Steinhauer (4, 5) give a useful description of the cratering process for aqueous and solvent-based paints. A local concentration of surface-active agent (low surface energy material), such as silicone oil contamination or a surfactant which was poorly dispersed within the paint, gives rise to a surface tension gradient (STG). Such low-surface-energy material may come into contact with the paint surface, either from the environment, e.g., airborne droplets of silicone oil contaminating an oven and so contacting a drying paint surface, or from within, e.g., droplets of one of the paint constituents reaching the surface.

The resulting surface shear stress drives a flow, in which the underlying viscous fluid is dragged away, leaving the crater. The observed diameter of the final craters varies from about 0.1 to 5 mm, and the time scale for their formation may be as little as 0.1 to 3 s (6). Generally the crater is much larger than the contaminated area causing the crater (4). Hahn identified several possible mechanisms that halt continued growth of a crater. The spreading surfactant may retract to form a liquid lens surrounded by a monolayer. When the contaminant is relatively soluble in the paint, it may be removed from the surface by solubilization, eliminating the driving surface tension gradient. Finally, if paint drying occurs rapidly enough, the resulting viscosity increase will inhibit further flow.

There are few published experimental studies of craters. The most relevant is that of Weh and Linde (3), who studied the craters produced by various silicone oils dissolved in xylene, either present as droplets within a coating that were allowed to rise to the surface or sprayed onto the surface. They performed experiments on coatings of pure solvents, on paint components, and on a clear lacquer paint, producing craters in coatings of 60–500 μm thick using drop volumes up to 0.01 μl. These craters were up to 1–2 mm across, appeared within minutes, and had both a developed rim and a small central peak. When drying of the coating was prevented, they found most craters were temporary features, due to leveling by capillarity and gravity. Other experimental works, by Ahmad and Hansen (7) and Gaver and Grotberg (8), studying the spreading of oleic acid on glycerine,

[1] To whom correspondence should be addressed. E-mail: schwartz@me.udel.edu.

0021-9797/00 $35.00

involved thicker films and spreading to large areas and are not especially relevant to the cratering seen in paint.

Numerical modeling of surfactant-driven flow in thin layers has been previously performed. Grotberg and Gaver (9) present a useful overview. Grotberg and co-workers (10–13) studied the flow of a thin layer of Newtonian fluid over a flat substrate, with insoluble surfactant on its surface. They derived a lubrication model similar to the one we will use here, including a nonlinear surfactant equation of state, for both two-dimensional and axisymmetric spreading. Their work was directed at measuring surfactant spreading rates, for medical applications such as drug delivery in the lung, and was less concerned with the changes to the free surface resulting from the flow. They found that when surfactant diffusion and capillarity are weak, an outward-moving wave forms, with a strong front or shock at the leading edge of the surfactant. This creates a large rim of material at the leading edge and thinning of the film behind it. Once the film becomes sufficiently thinned by STG-driven flow, van der Waals forces can become important (12), potentially leading to rupture of the film. Film rupture has been observed in experiments (14, 8) and simulations (15). Jensen and Grotberg (13) later extended their model to demonstrate that if the surfactant is able to dissolve into the underlying film, a large rim can be produced, where the film is temporarily three or more times thicker than the undisturbed film. This suggests that solubility may be a factor in producing high-rimmed paint craters.

Similarity methods (16, 12) have been used to identify solutions for STG-driven spreading opposed only by viscous forces, i.e., neglecting leveling by surface tension and gravity. In these circumstances, after suitable nondimensionalization, the evolution equations for film thickness h and surfactant concentration Γ reduce to

$$\frac{\partial h}{\partial t} = \frac{1}{r}\frac{\partial}{\partial r}\left(r\frac{h^2}{2}\frac{\partial \Gamma}{\partial r}\right), \qquad [1]$$

$$\frac{\partial \Gamma}{\partial t} = \frac{1}{r}\frac{\partial}{\partial r}\left(rh\frac{\partial \Gamma}{\partial r}\Gamma\right). \qquad [2]$$

Here r denotes distance from the drop center and t is the time since spreading began. The surfactant is insoluble and nondiffusive. Following Espinosa (16) and Grotberg and Jensen (12), a single similarity variable $\xi = r/t^a$ is sought which transforms the time-dependent partial differential equations [1] and [2] into ordinary differential equations. We rewrite the thickness and concentration as

$$h(r,t) = H(\xi); \qquad \Gamma(r,t) = G(\xi)/t^b.$$

Substituting, we find that [1] and [2] become equations in ξ alone only if $2a + b = 1$. The total amount of surfactant is conserved only if $2a - b = 0$. This requires $a = 1/4$ and $b = 1/2$. The equations then transform to

$$\xi\frac{dH}{d\xi} + \frac{2}{\xi}\frac{d}{d\xi}\left(\xi H^2\frac{dG}{d\xi}\right) = 0, \qquad [3]$$

$$\xi\frac{dG}{d\xi} + 2G + \frac{4}{\xi}\frac{d}{d\xi}\left(\xi HG\frac{dG}{d\xi}\right) = 0. \qquad [4]$$

A solution to [3] and [4] is

$$H = 2\left(\frac{\xi}{\xi_s}\right)^2; \qquad G = -\frac{1}{8}\log\left(\frac{\xi}{\xi_s}\right)$$

in $0 < \xi < \xi_s$. Here ξ_s is the location of a discontinuity at the outer edge of the spreading surfactant. The coating thickness jumps from 2 to 1, while the surfactant concentration reaches zero. At the center of the crater, the similarity solution has a film thickness of zero and infinite surfactant concentration. These boundary conditions are unrealistic, but the solutions obtained when leveling effects are weak are close to this one, except at the center and outer edge of the crater. A feature located at a particular value of ξ, such as the rim of the crater, has a position $r(t)$ which moves outward like $t^{1/4}$.

Espinosa *et al.* (17) have carried out similar numerical studies for spreading of surfactant inside a curved airway. Shen and Hartland (18) have performed numerical modeling of the disturbance caused by a local concentration of insoluble surfactant, assuming axisymmetry and based on lubrication theory. Schwartz *et al.* (19) derived a linear mathematical model and solved it for the time evolution of a thin liquid layer and the concentration of a surfactant covering it. Schwartz *et al.* (20) demonstrated use of finite difference and finite element methods to confirm the result obtained from the linear theory of the previous work, namely that surfactant retards leveling in general, but that, in certain circumstances, additional surfactant can augment leveling.

These works did not include evaporation and the subsequent viscosity increase, which are important in applications relevant to the coatings industry. Solvent evaporation rates during initial drying vary significantly and depend on the blend of solvents used, the air temperature and humidity, and the rate of airflow across the drying surface. For example, Stratta *et al.* (21) report evaporation rates between around 2×10^{-9} g/(cm^2 s) for a blend of phenyl ethyl ethers and 2×10^{-5} g/(cm^2 s) for methyl ethyl ketone, in still 25°C air. They found the evaporation rate for *n*-butyl acetate was about 14 times larger when drying air moved at 5 km/h compared to still air. They also performed simulations of the changes in solvent blends during drying for a uniform waterborne paint formulation. However, their model only considers compositional changes, so is unable to predict STG-driven flow.

Weidner *et al.* (22) presented a two-dimensional model for a two-component model paint composed of an evaporating solvent and a nonvolatile resin. A similar model was used by Howison *et al.* (23). Here the surface tension, evaporation rate, viscosity,

and surfactant diffusivity all depend on the local concentration of resin. Three-dimensional simulations were performed by Eres *et al.* (24) for an evaporating alkyd paint, for which STG effects are important. They also compared their results with a linearized theory for sinusoidal disturbances. They noted that a nonlevel wet paint layer can be made to produce a quite level dry surface if the evaporation rate is well chosen.

Welding is a related application in which surface tension gradients are caused by temperature differences across the surface of the molten weld pool. Dilute surface-active impurities may substantially alter these gradients (25). Numerical modeling (see, e.g., (26)) shows that the resulting flow pattern in the pool may be significantly modified. Laser direct writing (27) may also produce features similar to those presented here.

This work presents a model for crater formation resulting from surface tension gradients. The model allows study of the evolution of a thin liquid paint layer that has been covered with a nonuniform layer of surfactant. The surfactant can spread along the free surface of the paint layer due to liquid motion and diffusion. The paint drying process is modeled by including evaporation of a solvent within the paint and paint viscosification as the solvent is removed. Since craters are often approximately circular, an axisymmetric model is sufficient and is more convenient that a full three-dimensional model. The possibility of any circumferential variation, such as "fingering" (3, 28), is excluded here.

In the next section we derive a mathematical model for craters caused by surface tension gradients in an evaporating two-component mixture. The numerical method used to obtain solutions of the model equations is then outlined. Results of the numerical simulations of cratering are presented. We demonstrate how craters can be formed either by an initial concentrated quantity (a "bolus") of surfactant or by a source which continuously releases surfactant as it dissolves, such as a particle composed of surface-active material. The effects of changes in the strength of the mechanisms giving rise to the crater are considered, as are changes to the drying rate, surfactant diffusivity, and viscosification behavior of the paint. We also investigate the effect of a preexisting surfactant layer and find that such a layer reduces deformation of the paint surface caused by surfactant. We demonstrate that a simplified drying model produces the same crater features as the full model, while being more convenient to use. The final section summarizes our results and discusses implications for reducing cratering in paints.

2. DERIVATION OF A FLOW MODEL FOR CRATERING

We consider a thin layer of drying paint covering a flat substrate. We restrict ourselves to axisymmetric disturbances, so the thickness of the film at time t is $h(r, t)$, where r is radial distance measured along the substrate from the center of the disturbance and t is time. The coordinate perpendicular to the substrate is denoted by z. The paint layer is assumed to be a mixture of two components: a solvent, which is able to evaporate, and a resin, which cannot. This two-component model approximates the drying behavior of more complicated multicomponent paint mixtures. Because the paint layer is thin, it is assumed that there is sufficient diffusion within the layer that variations in resin concentration across the film thickness are much smaller than variations along the substrate. This allows the resin concentration to be considered independent of z, and so it is denoted $c(r, t)$. This "well-mixed" assumption has been defined rigorously elsewhere (22) . This assumption limits the present work to coatings that do not develop a pronounced "skin" as they dry. A multilayer extension of the present model could be formulated to treat a "skinning" coating.

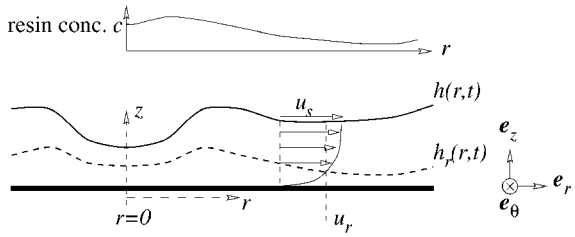

FIG. 1. The two-component paint, showing the coating thickness $h(r, t)$ and effective resin depth $h_r(r, t)$. The paint is assumed well mixed, with resin concentration $c = h_r/h$. The resin concentration $c(r, t)$ is shown here above the paint layer. At the free surface is a surfactant of concentration $\Gamma(r, t)$ (not shown).

It will generally be more convenient to refer to the effective "resin depth," $h_r(r, t) = c(r, t)\, h(r, t)$ rather than the resin concentration itself. The concentration of the surfactant (e.g., number of molecules per unit area) at the free surface is denoted by $\Gamma(r, t)$. Figure 1 shows the problem geometry.

The components of fluid velocity in the r and z directions are $u(r, z, t)$ and $v(r, z, t)$, respectively. The paint is assumed to be Newtonian, and its viscosity $\mu(c)$ is a sharply increasing function of the local resin concentration. The paint is sufficiently viscous that the flow is slow, and therefore liquid inertia may be neglected. The characteristic thickness of the film is H, while L is a substrate length scale, such as the size of the initial disturbance. Since the region of interest is long and thin ($H \ll L$), use of the lubrication approximation is appropriate. The paint surface tension σ depends only on the concentration of surfactant. The effects of gravity are neglected, so the pressure at the film surface only depends on the local surface tension and the free surface curvature. This is appropriate when the Bond number $\rho g L^2/\sigma \ll 1$. Here ρ is the paint density, assumed constant, and g the gravitational acceleration. For a typical crater $L \simeq 0.01$–0.1 cm, $\rho \simeq 1$ g/cm^3, and $\sigma \simeq 30$ dyn/cm so the Bond number is appropriately small. Neglecting inertia and gravity, and making the lubrication approximation, the governing equations are

$$\frac{\partial p}{\partial r} = \mu \frac{\partial^2 u}{\partial z^2}, \qquad [5]$$

$$\frac{\partial p}{\partial z} = 0, \qquad [6]$$

and the mass continuity equation is

$$\frac{1}{r}\frac{\partial}{\partial r}(ru) + \frac{\partial v}{\partial z} = 0. \quad [7]$$

The boundary conditions for [5]–[7] are: (i) The surface tension gradient at the free surface is balanced by the shear stress there, so

$$\mu\frac{\partial u}{\partial z} = \frac{\partial \sigma}{\partial r} \quad \text{at } z = h.$$

(ii) The no-slip boundary condition for a viscous fluid, on the substrate,

$$u = v = 0 \quad \text{at } z = 0.$$

(iii) Because the slope of the free surface is assumed small, an approximate form for its curvature may be used. Thus the pressure at the free surface is

$$p = -\sigma\nabla^2 h \quad \text{at } z = h.$$

Here the operator $\boldsymbol{\nabla}$ is the substrate gradient,

$$\boldsymbol{\nabla} = \boldsymbol{e}_r\frac{\partial}{\partial r} + \boldsymbol{e}_\theta\frac{1}{r}\frac{\partial}{\partial \theta},$$

measuring only variation in the radial direction. Integrating [5] in the z direction twice and imposing boundary conditions (i) and (ii) gives

$$\boldsymbol{u}(r, z, t) = \frac{1}{\mu}\left(\frac{1}{2}z^2 - hz\right)\boldsymbol{\nabla} p + \frac{z}{\mu}\boldsymbol{\nabla}\sigma, \quad [8]$$

indicating that the flow is driven by gradients in both pressure and surface tension. The pressure $p = p(r,\ t)$ is independent of z. Integrating across the paint thickness gives the flux

$$\boldsymbol{Q}(r, t) = \int_0^{h(r,t)} \boldsymbol{u}(r, z, t)\, dz = -\frac{h^3}{3\mu}\boldsymbol{\nabla} p + \frac{h^2}{2\mu}\boldsymbol{\nabla}\sigma. \quad [9]$$

The solvent evaporation rate $e(c)$, which has the units of speed, is assumed to depend only on the local resin concentration c at each location. The mass conservation equation [7] for the liquid can be integrated to yield

$$\frac{\partial h}{\partial t} = -\boldsymbol{\nabla}\cdot\boldsymbol{Q} - e(c). \quad [10]$$

Combining [9] and [10] gives an evolution equation for film thickness,

$$\frac{\partial h}{\partial t} = -\boldsymbol{\nabla}\cdot\left[\frac{h^3}{3\mu}\boldsymbol{\nabla}(\sigma\nabla^2 h) + \frac{h^2}{2\mu}\boldsymbol{\nabla}\sigma\right] - e(c), \quad [11]$$

where $\mu = \mu(c)$ and $\sigma = \sigma(\Gamma)$.

Because the resin component is assumed to be well mixed, it is simply carried along with the total liquid mixture. The outward flux of resin is therefore $\boldsymbol{Q}_r = c\boldsymbol{Q}$. The resin component does not evaporate, so its evolution is given by

$$\frac{\partial h_r}{\partial t} + \boldsymbol{\nabla}\cdot(\boldsymbol{u}_r h_r) = 0, \quad [12]$$

where the advective resin velocity is the thickness-averaged total velocity, $\boldsymbol{u}_r = \boldsymbol{Q}/h$. Because the layer is thin, resin transport by diffusion in the radial direction is small compared to advective transport.

The concentration of surfactant at the surface satisfies

$$\frac{\partial \Gamma}{\partial t} + \boldsymbol{\nabla}\cdot(\boldsymbol{u}_s\Gamma) = D_s\nabla^2\Gamma - D_b(\Gamma - \Gamma_b)h + q_\Gamma, \quad [13]$$

where $\boldsymbol{u}_s$, the liquid velocity at the free surface, is found from [8]:

$$\boldsymbol{u}_s = \boldsymbol{u}|_{z=h} = -\frac{h^2}{2\mu}\boldsymbol{\nabla} p + \frac{h}{\mu}\boldsymbol{\nabla}\sigma.$$

D_s is the surfactant diffusivity, assumed constant. The term involving D_b is intended to model bulk transfer of surfactant between the surface and the film interior if the local surfactant concentration differs from some "reservoir" value Γ_b. At equilibrium there is a fixed relationship between the concentration of a soluble surfactant in the bulk of the film and the amount adsorbed at the surface, described by an adsorption isotherm (29). Thinner parts of the film become saturated with surfactant more quickly than thicker parts, which tends to maintain higher surfactant levels in the thin parts of the film. This accentuates the surface tension gradients that drive the flow. The final term, q_Γ is a surfactant supply rate that is used to model release of surfactant from a local source.

Closure of the model requires expressions for the viscosity and evaporation rate as functions of c and the surface tension as a function of Γ. For the viscosity, the power law

$$\frac{\mu(c)}{\mu_0} = (1 + B)\left(\frac{c}{c_0}\right)^M - B \quad [14]$$

is chosen, where B and M are positive constants so that, as the paint becomes more resin-rich, its viscosity increases. μ_0 is the viscosity $\mu(c_0)$ at the initial concentration c_0. The evaporation rate is assumed to be constant until the mixture is dry, i.e.,

$$e(c) = \begin{cases} e_0 & \text{for} \quad c < c_{\text{dry}} \\ 0 & \text{for} \quad c \geq c_{\text{dry}} \end{cases}. \quad [15]$$

An important specification is the surface tension equation of state. Earlier studies of STG-driven flow often approximated this as linear, but the surfactants in paints cause large reductions, and

at high concentrations a linear law may imply negative surface tensions. Instead we use the law

$$\sigma(\Gamma) = (\sigma_0 - \sigma_\infty)\frac{\sqrt{1+\chi^2}-\chi}{\sqrt{1+\chi_0^2}-\chi_0} + \sigma_\infty,$$
$$\chi = A(\Gamma - \Gamma_1), \qquad \chi_0 = -A\Gamma_1, \tag{16}$$

where σ_0 is the surface tension of the clean (surfactant-free) coating and σ_∞ is the minimum surface tension, occurring at large surfactant concentrations. The value of Γ_1 represents the critical micelle concentration (see (29)) above which the surface tension is nearly independent of concentration. The value of Γ_1 sets the location of the "kink" in [16]. At low surfactant levels, the surface tension decreases nearly linearly, behaving like

$$\sigma(\Gamma) = \sigma_0 - (\sigma_0 - \sigma_\infty)\frac{\Gamma}{\Gamma_1}.$$

Sheludko (30) has proposed a dependence of surface tension on surfactant concentration similar to that of [16].

The three evolution equations for h, h_r and Γ, with the above expressions, make up the full cratering model.

3. NONDIMENSIONALIZATION AND NUMERICAL METHOD

The evolution equations [11], [12], and [13] are nondimensionalized before we attempt to solve them. Film thickness h and resin thickness h_r are nondimensionalized using the thickness H of the initial undisturbed wet layer. Lengths along the substrate are referenced to the length scale of the initial contamination, L. The dimensionless surface tension σ^* is defined by

$$\sigma(\Gamma) = (\sigma_0 - \sigma_\infty)\sigma^*(\Gamma^*) + \sigma_\infty,$$

where $\Gamma^* = \Gamma/\Gamma_1$ is the dimensionless surfactant concentration. The dimensionless surface tension thus varies between 0 at large surfactant concentrations and 1 for a surfactant-free surface. Viscosities are related to the initial value μ_0. The time scale is taken to be that for leveling by surface tension of a disturbed layer (31), which is

$$T = \frac{3\mu_0 L^4}{\sigma_0 H^3}.$$

Rewriting [11], [12], and [13], in dimensionless variables, and dropping the stars on σ^* and Γ^*, they become

$$\frac{\partial h}{\partial t} = -\frac{1}{r}\frac{\partial}{\partial r}(rQ) - E, \tag{17}$$

$$\frac{\partial h_r}{\partial t} = -\frac{1}{r}\frac{\partial}{\partial r}\left(r\frac{Q}{h}h_r\right), \tag{18}$$

$$\frac{\partial \Gamma}{\partial t} = -\frac{1}{r}\frac{\partial}{\partial r}(ru_s\Gamma) + \delta\frac{1}{r}\frac{\partial}{\partial r}\left(r\frac{\partial \Gamma}{\partial r}\right) - \delta_b(\Gamma - \Gamma_b)h + Q_\Gamma. \tag{19}$$

Each is in divergence form, as this enables use of numerical methods which automatically conserve h, h_r and Γ. The fluxes are

$$Q = \frac{h^3}{\mu}\frac{\partial}{\partial r}\left(\frac{1}{r}\frac{\partial}{\partial r}\left[r\frac{\partial h}{\partial r}\right]\right) + A\frac{h^2}{\mu}\frac{\partial \sigma}{\partial r}, \tag{20}$$

$$u_s = \frac{3}{2}\frac{h^2}{\mu}\frac{\partial}{\partial r}\left(\frac{1}{r}\frac{\partial}{\partial r}\left[r\frac{\partial h}{\partial r}\right]\right) + 2A\frac{h}{\mu}\frac{\partial \sigma}{\partial r}, \tag{21}$$

where the nondimensional parameters are

$$A = \frac{3}{2}\frac{\sigma_0 - \sigma_\infty}{\sigma_0}\left(\frac{L}{H}\right)^2, \qquad E = \frac{Te_0}{H},$$
$$\delta = \frac{TD_s}{L^2}, \qquad \delta_b = TD_bH.$$

A is an aspect ratio, with larger values indicating that surface tension gradients will have a more significant effect. The drying parameter E is a measure of the dimensionless time to dry a uniform layer of paint, T_d. For a constant evaporation rate of e_0,

$$T_d = \frac{(1-c_0)H}{e_0 T} = \frac{(1-c_0)}{E}.$$

Because both evaporation rate and paint viscosity may vary considerably, E may vary over a wide range. δ is a diffusion parameter, and δ_b is a bulk diffusion parameter. The dimensionless surfactant source function is $Q_\Gamma = (T/\Gamma_1)q_\Gamma$. In obtaining Eqs. [20] and [21] from Eq. [8], variation in $\sigma(\Gamma)$ has been neglected in the leveling terms, since it is dominated by the surface tension gradient term when $H \ll L$, as discussed in Ref. (24).

A finite-difference numerical method is used to solve the coupled nonlinear equations governing h, h_r, and Γ. The spatial domain $0 \le r \le L_\infty$ is discretized into $(N+1)$ cells. Defining the grid spacing, $\Delta r = L_\infty/(N+1/2)$, we replace the continuous function $h(r,t)$ by the discrete quantities $h_i^{(k)} \equiv h(r_i, t_k)$, where $r_i = i\,\Delta r$ for $i = 0, 1, \ldots, N$. Similarly we define discretized resin $h_{r_i}^{(k)}$ and surfactant $\Gamma_i^{(k)}$. At $r = 0$ the limiting forms of the equations as $r \to 0$ are applied, along with no-flux conditions. No-flux conditions are also imposed at the outer boundary point at $r = L_\infty$, which is chosen to be far enough from the center to provide minimal interference to the solution.

At each time step, the discretized equations are solved as follows:

1. Find the new height field, $h_i^{(k+1)}$. Differencing the fourth-order derivative at the new time level leads to an implicit method, in which the unknown values $h_i^{(k+1)}$ are interrelated by a set

of coupled equations. Finding these unknown $h_i^{(k+1)}$ from the known $h_i^{(k)}$ requires solving a pentadiagonal system of $(N+1)$ linear equations. While an explicit method would not require solution of a linear system because the $h_i^{(k+1)}$ are not coupled, it would require an excessively small time step, and hence many iterations, for stability. The implicit method is unconditionally stable (32) for the model biharmonic equation

$$\frac{\partial \phi}{\partial t} = -\frac{\partial^4 \phi}{\partial x^4},$$

so much larger time steps can be used than if an explicit method were used.

2. Find the new surfactant field, $\Gamma_i^{(k+1)}$. First the surface speeds $u_s|_{i-1/2}$ are found using the newly determined $h_i^{(k+1)}$ field, but surfactant values are evaluated at the previous time step. The advective term is handled implicitly, while the remaining terms are explicit. A tridiagonal linear system of equations is then solved.

3. Find new resin depth field, $h_{r_i}^{(k+1)}$. This requires calculation of the thickness-averaged speed, $(Q/h)_{i-1/2}$, using the new values of $h_i^{(k+1)}$ and $\Gamma_i^{(k+1)}$. The advective term is treated implicitly, so a tridiagonal linear system must again be solved.

At this point, the new resin concentration, surface tensions, evaporation rates, and viscosity are calculated and the next time step begins. The simulation ends either when a specified minimum concentration ($c \simeq c_{\mathrm{dry}}$, say) is obtained at all grid points or at a specified final time. The initial action of the surfactant is very fast, while the subsequent leveling and evaporation are slower. Due to this difference in time scales, the time stepping is adaptive, with a larger time step used as changes in the solution become smaller.

4. RESULTS

The mathematical model is used to simulate craters driven by two different mechanisms. In the first, a finite amount of surfactant is placed on the film surface. In the second, a localized surfactant source steadily releases surfactant at constant rate over a small portion of the paint layer. These two mechanisms are examined in turn, along with the effects of changing their strengths and the values of the parameters E, δ, δ_b, and M. We consider the way in which a small amount of preexisting surfactant may lead to less pronounced craters. Finally, we present a variant of our model which treats the drying process in a simplistic fashion, yet produces qualitatively similar craters.

The parameters chosen are thought to be representative of real craters. However, the published literature contains few quantitative details of cratering, so some improvisation is required. Throughout this section we study the cratering of a hypothetical paint with the properties given in Table 1 as a base case. The characteristic leveling time obtained from these values is $T = 7.2$ s. The dimensionless aspect ratio is $A = 37.88$. The drying rate is chosen so that drying is complete after 10 min, and the corresponding drying parameter is $E = E_0 = 4.8 \times 10^{-3}$. Drying was considered complete when the resin concentration $c > c_{\mathrm{dry}} = 0.995$ everywhere. Reported values of surfactant diffusivity [8] lie in the range

$$1 \times 10^{-6}\,\mathrm{cm^2/s} < D_s < 1 \times 10^{-4}\,\mathrm{cm^2/s}.$$

Choosing an intermediate value, 8.6×10^{-6} cm^2/s, gave $\delta = 0.1$. Except where otherwise noted, these values were used throughout.

TABLE 1
Base Properties of the Fictitious Paint Used for Simulations

Property, symbol	Value
Initial film thickness, H	30 μm
Horizontal length scale, L	0.025 cm
Initial resin fraction, c_0	0.6
Reference surface tension, σ_0	30 dyn/cm
Minimum surface tension, σ_∞	22 dyn/cm
Surface tension law "kink", A	10
Surfactant diffusivity, D_s	8.6×10^{-6} cm^2/s
Initial paint viscosity, μ_0	5 P
Viscosity law constant, B	4
Viscosity law constant, M	25
Drying time, $T_d T$	600 s
Drying rate, e_0	2.0×10^{-6} cm/s

4.1. Localized Surfactant Concentrations

We first simulated cratering in a drying paint layer produced by a localized mass or "bolus" of surfactant centered at $r = 0$. The simulation began with an initially flat layer of paint with uniform dimensionless thickness $h = 1$ and resin concentration $c = c_0$, with an initial dimensionless surfactant distribution given by

$$\Gamma(r, 0) = \frac{\Gamma_0}{1 + (r/L)^{10}}. \qquad [22]$$

This initial surfactant profile has an abrupt drop in surfactant concentration, from Γ_0 to zero, at $r = L$. There is a large initial surface tension gradient in this region, which drives the subsequent flow. In addition to the paint and surfactant properties stated above, the bolus concentration was $\Gamma_0 = 1$, and the bulk diffusion of surfactant was neglected ($\delta_b = 0$). The outer boundary was placed $20L$ (0.5 cm) from the center. With 100 grid points, about 5 min was required on a Pentium II personal computer until the paint was dry everywhere.

The formation of a crater arising from the surfactant-driven flow is shown in Fig. 2. The initial flow is driven by the gradient in surface tension, which creates an outward flow. This produces a disturbance in the free surface, which rapidly grows in amplitude. At the same time, surfactant is carried outward by the flow, and so the disturbance also spreads outward. It is eventually halted by drying. The height of the crater rim above the

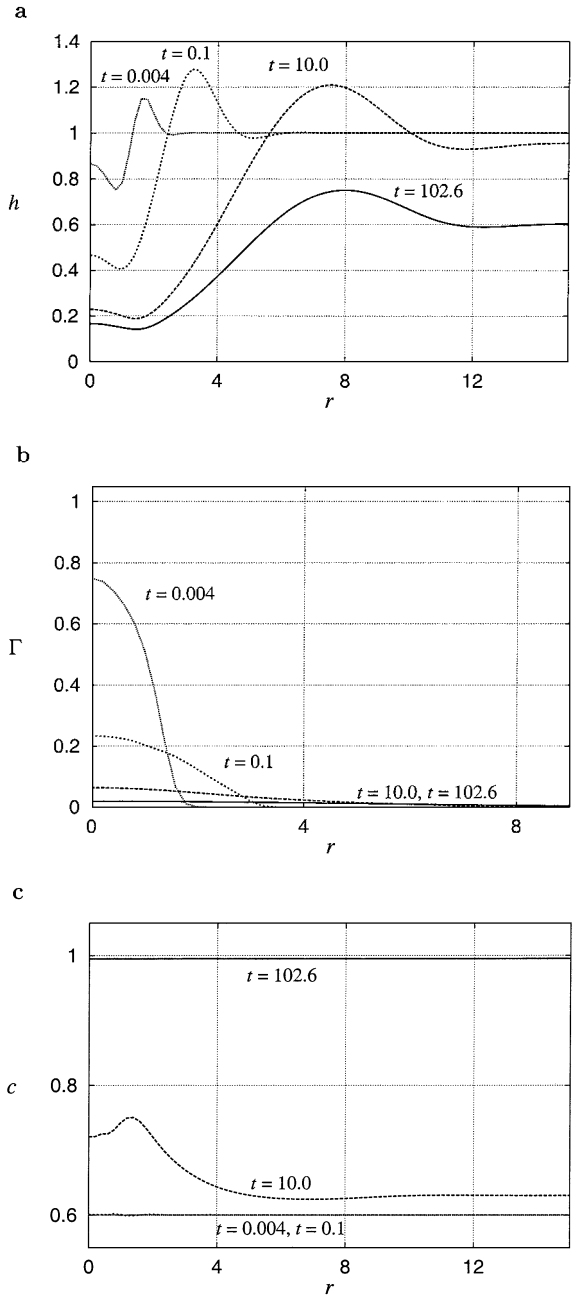

FIG. 2. Evolution of a crater in the paint described in Table 1, driven by a localized initial surfactant bolus with concentration given by [22] and $\Gamma_0 = 1$, shown at several dimensionless times: (a) coating thickness h, (b) surfactant Γ, (c) resin concentration c. The simulation begins with a flat paint layer. A disturbance created by the initial gradient in surface tension rapidly grows in amplitude and spreads outward until halted by drying. The paint is dry at $t = 102.6T$ (742 s). The vertical scale showing coating thickness in this and subsequent figures has been greatly exaggerated.

undisturbed fluid far from the disturbance reaches a maximum around $t = 3.6$ s ($0.5T$). Because the time scales for STG-driven flow and evaporation greatly differ, nearly all of the crater growth occurs in the first few seconds, but it takes a long time for evaporation to remove all the remaining solvent. Thinning of the layer near the center of the defect by STG-driven flow, in combination with solvent removal at a constant evaporation rate, causes resin concentration to increase most rapidly there (see Fig. 2c). The paint first dries at $t \simeq 140$ s ($20T$), near the center at $r = 1.5L$, while a uniform paint layer would not dry until $t = T_d = 600$ s ($83.3T$). The slowest part to dry is the crater rim, where a relatively thick coating is created. Drying is not complete here until $t = 742$ s ($102.6T$). The thickest part of the crater rim is at a radius of about $8L$, corresponding to a diameter of about 4 mm. Figure 3 shows the final crater in perspective form, in which the pronounced rim and central hump are clearly visible. These features correspond to those seen in the crater profile measured by Weh and Linde (3).

If the airflow past a drying coating is controllable, such as in a dryer, then the drying parameter E may be varied without modifying the coating. While an increase in E is most obviously seen as an increase in evaporation rate, E also increases with viscosity, and with L^4. Fig. 4a illustrates how increasing the drying rate leads to a smaller final crater with a steeper wall, while decreasing E causes a broader crater. For instance, a 10-fold increase in drying rate, corresponding to drying of a uniform coating in 60 s, leads to a halving of the crater radius. Decreasing E reduces the height of the central peak of the crater. This is because slower evaporation rates (smaller E) require longer drying times, so there is more time for spreading and leveling to occur after the initial crater creation. Using the similarity scaling $\xi = x/t^{1/4}$ previously identified (16, 12) as appropriate for radial spreading of a surfactant on a thin film, as described in the Introduction, the data used in Fig. 4a were rescaled using the time t_{dry} at which the coating became dry everywhere, for each value of E. The crater rim was always the last part of the model domain to dry. For the $E = 10E_0$ case t_{dry} was $10.4T$ (i.e., 75 s), while for $E = 0.1E_0$ it was $998T$ (7190 s). Apart from near the crater center, $\xi < 1$, the results for different drying rates collapse onto the same curve (see Fig. 4b). Since this similarity result was obtained for a nonevaporating, constant viscosity thin film, this suggests that evaporation has only a slight effect on the shape of a bolus-driven crater, other than establishing a stopping time for crater formation. This idea is examined further in Section 4.4.

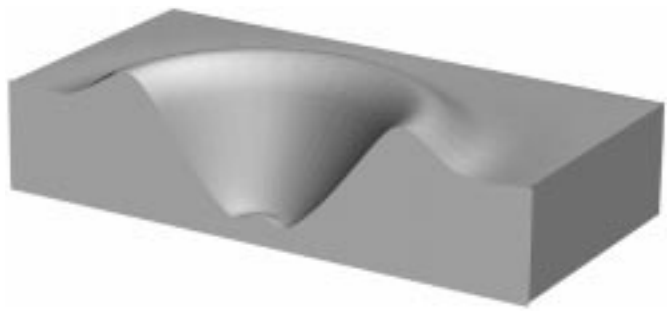

FIG. 3. Rendered cut-away view through the center of a bolus-driven crater in a paint with the properties given in Table 1. This is the final free surface profile as shown in Fig. 2a, illustrating the central peak and crater rim.

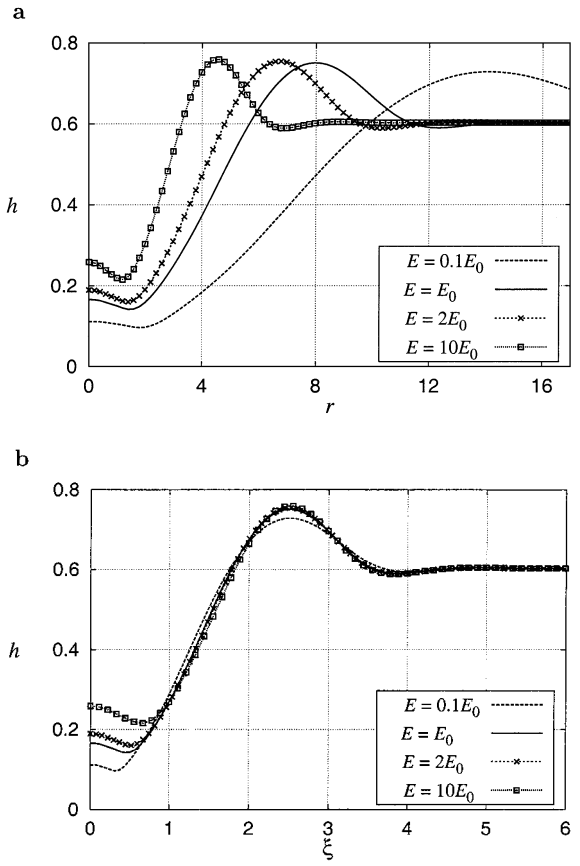

FIG. 4. Effect of varying drying parameter E, between 0.1 and 10 times its original value, on the final coating thickness h for the bolus-driven crater in Fig. 2. Rapid drying (large E) limits flow in the paint layer, resulting in a smaller and shallower crater. In (a) the horizontal coordinate is r; in (b) it is $\xi = r/t_{\mathrm{dry}}^{0.25}$, demonstrating similarity. In each case, drying is complete at $t = t_{\mathrm{dry}}$. Initial surfactant distribution is given by [22] with $\Gamma_0 = 1$.

Since the surfactant bolus is responsible for the crater, variation of the concentration and shape of the initial bolus may have a substantial effect on the subsequent crater. As Γ_0 is increased, the final dry crater produced becomes both broader and deeper, including a larger crater rim. For large Γ_0, the narrow neck around $r = 2L$ restricts flow between the central peak of the crater and the surrounding fluid. For craters with a larger initial concentration ($\Gamma_0 > 3$) an extremely thin region forms at $r \simeq 2L$, leading to numerical difficulties. In reality we expect that once the film becomes extremely thin (on the order of several μm) intermolecular forces will become important (33, 34), causing rupture here and creating an annular patch of exposed substrate as observed previously (3, 8). Such effects are not considered here. We also investigated the effect of altering the shape of the surfactant distribution, without changing the total amount of surfactant. The Gaussian initial surfactant distribution

$$\Gamma(r, 0) = \Gamma_0 \exp\{-(r/L)^2\} \qquad [23]$$

contains approximately the same amount of surfactant but is considerably smoother than [22]. The total amount of surfactant added is $M_\Gamma = \int_0^\infty \Gamma(r, 0)(2\pi r)\, dr$. For the distribution represented by [22], $M_\Gamma = 1.068\pi\Gamma_0$ while for [23] it is similar, $M_\Gamma = \pi\Gamma_0$. Figure 5 shows results for several drying rates using initial condition [23] with $\Gamma_0 = 1$. Comparison with Fig. 4a shows that the resulting final profiles are generally similar except at the center of the crater. This suggests that the general size and depth of the crater are insensitive to the exact shape of the initial surfactant bolus. However, the small peak seen at the center in Fig. 4a is no longer seen, so this feature, often seen in real craters, may depend on the specific distribution of surfactant at the site of contamination. We also simulated the crater resulting from an initial surfactant given by [22] but with L doubled and Γ_0 correspondingly reduced to 0.25, giving the same $M_\Gamma = 1.068\pi\Gamma_0$. The outer part of the crater at each time and the final profile obtained are again very similar to those shown in Fig. 4a. There are differences in the inner part ($r < 4L$), however, with the broader surfactant distribution causing less thinning at the crater center. The total amount of surfactant in the bolus M_Γ appears important in establishing the size of the resulting crater, with the local distribution determining its inner profile.

Figure 6 shows the result of changes in surfactant diffusivity. The final dry h is only altered minimally, with a slight smoothing evident at the crater rim, but there are prominent changes in surfactant. Surfactant is largely confined to the crater when there is little diffusion, but moves well outside when δ is larger. Figure 7 shows that bulk diffusion has a more appreciable effect on the final coating profile, tending to "focus" the crater, with a smaller radius but steeper rim. The equilibrium surfactant concentration Γ_b was zero. The bulk diffusion term therefore is a sink for surfactant, opposing the surfactant source term which creates the crater. Plots of the surfactant concentration distribution show that when δ_b is nonzero, the surfactant is almost entirely removed from the surface outside the crater rim, eliminating any surface tension gradient there.

The "solidifying rate" of the paint has a large effect on the shape of the final defect. When M is small, there is little increase

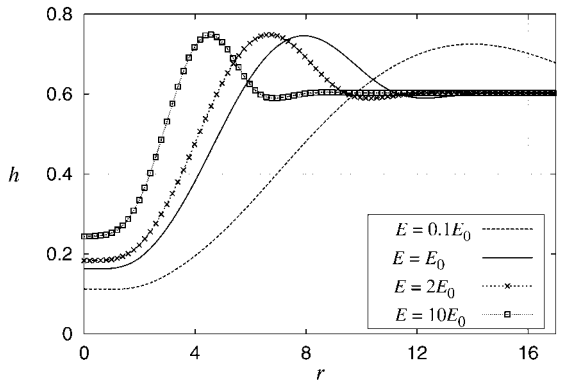

FIG. 5. Effect of varying drying parameter E, between 0.1 and 10 times its initial value, on the final coating thickness h of a bolus-driven crater with the Gaussian initial surfactant profile [23] and $\Gamma_0 = 1$. The smoother initial condition leads to craters which do not have the inner bump seen in Fig. 4a. However, the outer shape of the craters is not significantly altered.

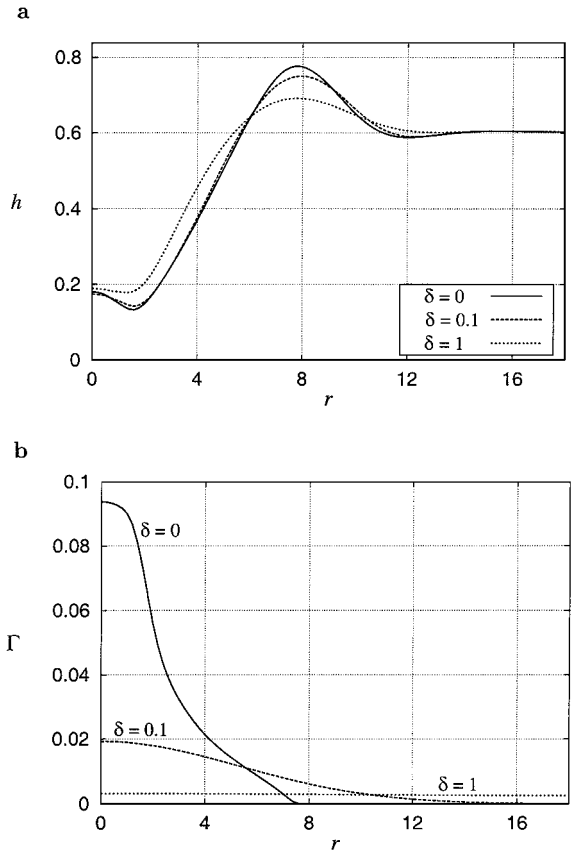

FIG. 6. Effect of varying surfactant diffusivity parameter δ between 0 (no diffusion) and 1 on the bolus-driven crater in Fig. 2. (a) As diffusion is increased, the crater rim height is reduced. (b) Surfactant spreads across the entire surface due to diffusive transport, while without surfactant diffusion it is transported only by outward motion of the free surface.

in paint viscosity as the solvent is removed during drying. Accordingly, Fig. 8 shows that craters become broader as M is reduced. In particular, the central peak is less developed, perhaps because of enhanced leveling. Because of the extent of the

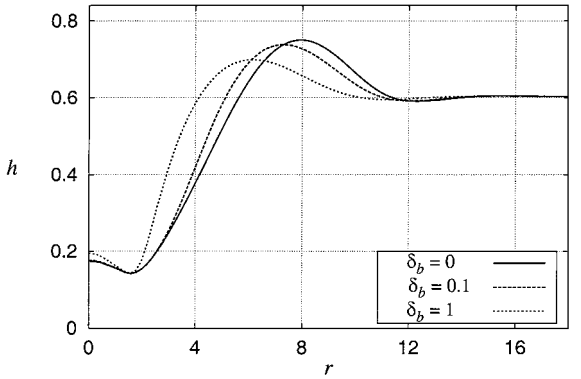

FIG. 7. Effect of varying surfactant bulk diffusivity parameter δ_b between 0 (no bulk diffusion) and 1 on final coating profile h, for the bolus-driven crater in Fig. 2. Bulk diffusion removes surfactant from the surface, reducing surface tension gradients, and so leads to less pronounced craters.

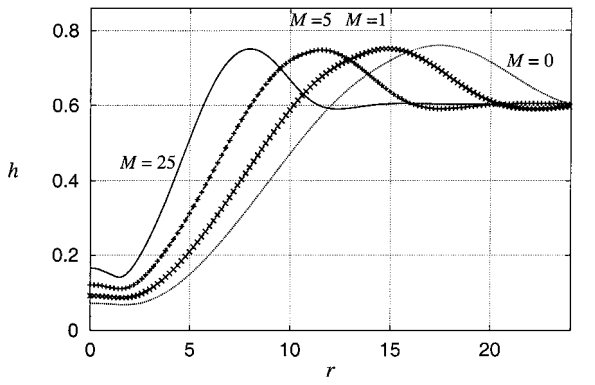

FIG. 8. Effect of varying viscosification exponent M between 0 (constant viscosity) and 25 on the final coating profile h for the bolus-driven crater in Fig. 2. Large M means that the paint viscosity increases rapidly as solvent is removed during drying. This restricts flow of paint away from the crater site, producing a smaller crater.

spreading, here we extended the domain so 150 grid points were used with $L_\infty = 30$. $M = 0$ corresponds to the case of a paint with constant viscosity, such as one which is prevented from drying. More substantial cratering in this case is consistent with the results of Weh and Linde (3), who observed a higher crater density (per unit of covered area) when viscosity was reduced by thinning and when evaporation was prevented.

4.2. Localized Surfactant Sources

The model also allows investigation of the drying of a paint layer subject to a steady source of surfactant. The source, centered at $r = 0$, is of the form

$$Q_\Gamma(r) = Q_s \exp\{-(r/L)^2\}, \qquad [24]$$

where L is the length scale for the source. The source itself does not spread. Simulations began with an initially uniform and surfactant-free paint layer, with $h = 1$, $c = c_0$ and $\Gamma = 0$ everywhere, with the same paint properties and numerical details as for the surfactant bolus in the previous section. The dimensionless surfactant source strength was $Q_s = 0.01$.

The changing thickness profile and surfactant and resin concentration are shown in Figs. 9a, 9b, and 9c. Most of the crater formation is completed by about $t = 72$ s ($10T$), before evaporation has had much effect. Later development is dominated by evaporation, with relatively little change in the shape of the free surface, due to the rapidly increasing paint viscosity. The surfactant is transported outward by both STG-driven flow and surfactant diffusion, which spreads a low concentration of surfactant over the entire domain. The inner part of the surfactant distribution is dominated by the shape of the source described by [24]. Surfactant concentration at the crater center steadily increases, in contrast to the bolus-driven crater. Thus the growth of the crater is less abrupt than that for a bolus-driven crater. As for the bolus-driven craters, concentration of resin increases most rapidly in the central region. Accordingly, central parts of the

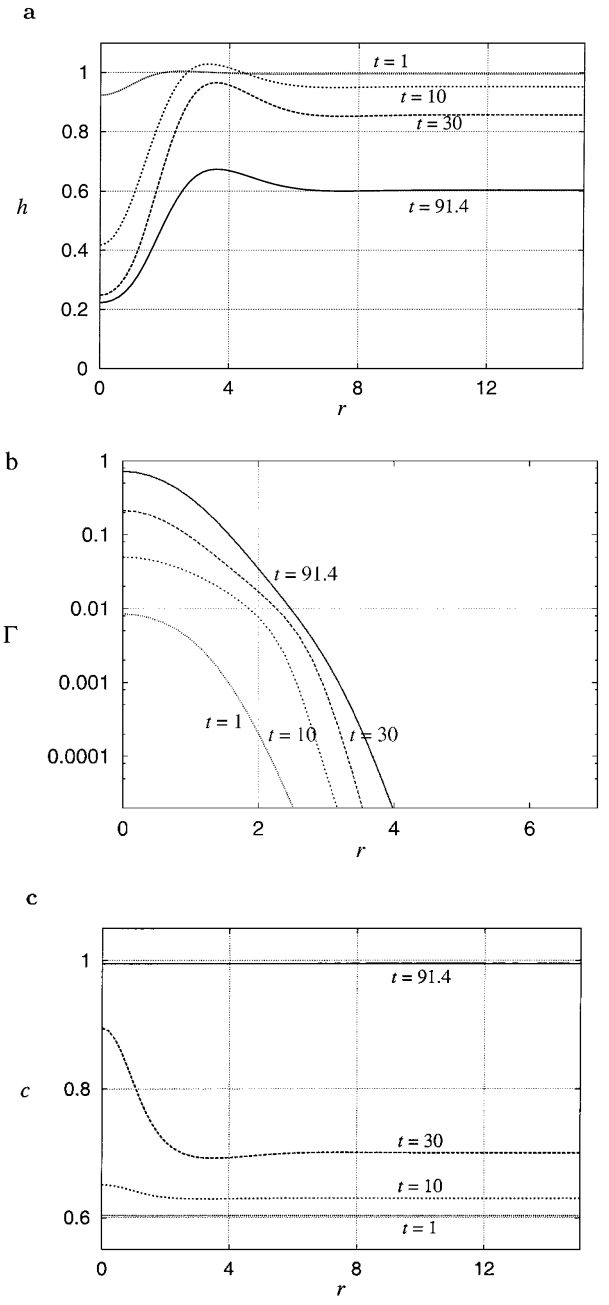

FIG. 9. Evolution of a crater in the paint described in Table 1, driven by a surfactant source of strength $Q_s = 0.01$ described by [24], shown at several dimensionless times: (a) coating thickness h, (b) surfactant Γ, (c) resin concentration c. The paint layer is initially flat and free of surfactant. The crater grows gradually as surfactant is continually added. At $t = 91.4T$ (661 s) the paint is dry everywhere, leaving a permanent crater in the coating.

crater are the first to dry, around $t = 260$ s ($36T$). The time to dry everywhere is 661 s ($91.4T$), slightly longer than an undisturbed surfactant-free layer, which would have required 600 s to dry.

As before, the drying parameter has a substantial effect on the final crater profiles. Figure 10 shows that increasing the evaporation parameter E results in a smaller, shallower crater. This is

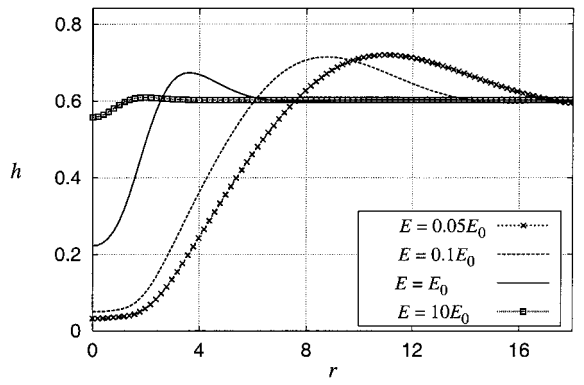

FIG. 10. Effect of varying drying parameter E between 0.05 and 10 times the original value on the final coating profile h, for the source-driven crater in Fig. 9. The surfactant source strength $Q_s = 0.01$. As for the surfactant bolus (see Fig. 4), slower drying, or reduced initial viscosity, allows a larger crater to form.

because less time is available for the source to release surfactant, so only modest surface tension gradients are created, and there is therefore little outward flow to excavate material. Because the quantity of surfactant present is no longer fixed, the profiles obtained for the various drying rates do not collapse under the similarity transformation used for bolus-driven craters.

If the surfactant supply rate Q_s is increased, a more pronounced crater is produced. Figure 11 shows the final profiles produced by several dimensionless surfactant supply rates. The defects produced vary from a small depression for $Q_s = 0.001$, to a deep crater which nearly dewets for $Q_s = 1$. For strong sources, nearly all the liquid at the center is removed. In practice, Q_s would be determined by comparison with experiment. Comparison of Figs. 10 and 11 indicates that decreasing evaporation rate and increasing surfactant supply rate have similar effects, both increasing the severity of cratering. This observation suggests that the total amount of surfactant added, approximately $Q_s T_d$, i.e., proportional to (Q_s/E), may be of importance in determining whether a severe crater will form.

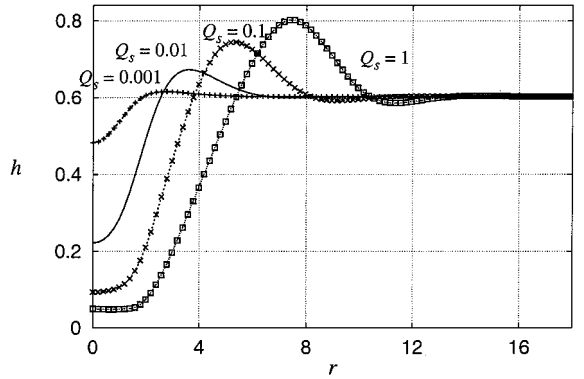

FIG. 11. Effect of varying surfactant supply rate Q_s from 0.001 to 1 on the final coating profile h, for the source-driven crater in Fig. 9. The surfactant source is described by [24]. Faster release of surfactant leads to more severe cratering.

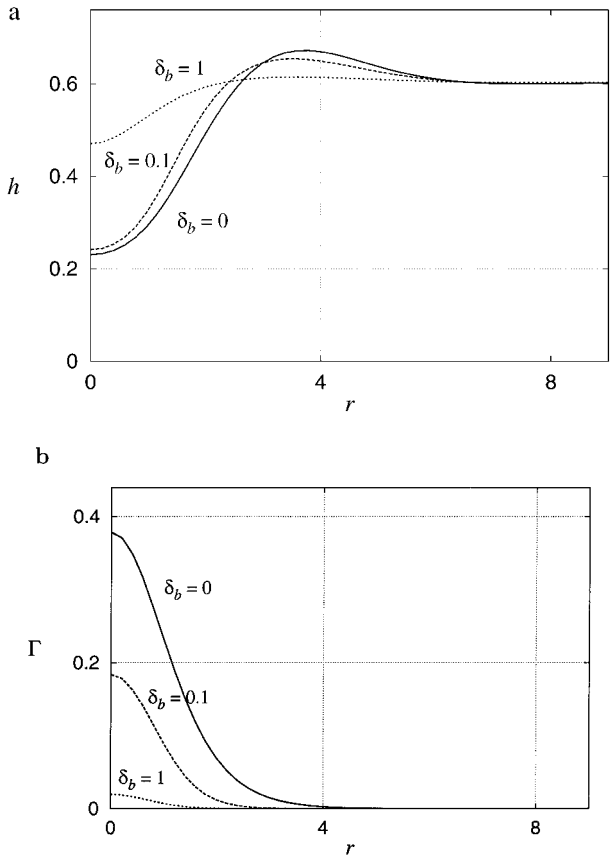

FIG. 12. Effect of varying surfactant bulk diffusivity parameter δ_b between 0 (no bulk diffusion) and 1 on (a) final coating profile h, (b) final surfactant distribution Γ, for the source-driven crater in Fig. 9. Here the surfactant source strength is $Q_s = 0.01$, and the source is described by [24]. Introducing surfactant bulk diffusion diminishes the crater, by providing a sink, removing surfactant from the paint surface.

Surfactant diffusivity has only a modest effect on the final crater shape, similar to that seen in the previous section for bolus-driven craters. With increased surfactant diffusion, surfactant spreads more evenly across the film, reducing surface tension gradients. Both the depth of the crater and the height of the rim are therefore somewhat reduced. The effect of introducing bulk diffusion can be seen in Fig. 12. The final dry coating profiles are shown for various values of the bulk diffusion parameter δ_b. As before, the equilibrium surfactant concentration Γ_b was set to zero, so the bulk diffusion term acts as a sink for surfactant. The result is a less developed defect in the dry coating. Figure 12b shows that the final concentration of surfactant left on the paint surface once it is dry is greatly reduced when there is bulk diffusion. This is presumably similar to what would be observed for a surfactant which is soluble in the paint.

Changes in the viscosity-concentration law have an effect similar to that described in the previous section. Reducing M results in a broader crater, with a higher rim. The resulting family of craters is quite similar to those produced by varying surfactant supply rate (see Fig. 11). For small M there is nearly complete removal of material at the center. This is in contrast to the bolus-driven craters, for which the central film thickness is not markedly reduced as M is lowered.

4.3. Preexisting Surfactant

Lowering the surface tension of a coating is a commonly suggested remedy to prevent cratering (2, 4, 5), such as by adding a soluble surfactant (6). In this section we demonstrate that by providing a coating with a small but uniform amount of the surfactant responsible for cratering, the extent of craters caused by inevitable contamination may be reduced. Such a layer might arise from the deliberate addition of surfactant or as a result of previous cratering in the paint. The enhanced leveling effect of surfactant on a nearly uniform layer with surfactant has been noted by Schwartz *et al.* (19, 20). Simulations demonstrating reduced spreading when there is preexisting surfactant have been performed, e.g., (17).

The initial surfactant distribution is modified by beginning with a small uniform amount of surfactant Γ_∞ on the entire surface, in addition to either a local concentration or source. For bolus-driven craters, the initial surfactant is described by

$$\Gamma(r, 0) = \Gamma_\infty + \frac{\Gamma_0}{1 + (r/L)^{10}}, \qquad [25]$$

while for source-driven craters, there is already surfactant present when the simulation starts.

The bolus-driven crater simulation presented in Fig. 2 was repeated with varying levels of ambient surfactant. Figure 13a shows the final crater profiles for each value of Γ_∞ and indicates that the severity of the crater lessens as Γ_∞ is increased. The crater radius is reduced, and the thinning near the center is less severe. Figure 13b indicates that surfactant spreads further when there is already surfactant present. Thus the region in which there are appreciable gradients in surface tension extends to larger r. During the simulation with $\Gamma_\infty = 0.5$, the coating thickness at the center $h(0, t)$ was seen to increase for a period of time after the initial crater development, but before drying was complete. This indicates that back-flow due to leveling is sufficiently strong to overcome the general decrease in film thickness due to evaporation. Figure 14 shows the corresponding results for the source-driven crater shown in Fig. 9 but with preexisting surfactant. The resulting final profiles show less severe cratering for nonzero Γ_∞.

With the same range of evaporation rates as that used to produce Fig. 4, the runs shown there were repeated for a bolus-driven crater, the only change being the addition of a preexisting surfactant layer of concentration $\Gamma_\infty = 0.1$. The resulting final profiles show significant attenuation of the craters, compared to Fig. 4, particularly when drying is slow. Unlike the self-similar spreading seen in Fig. 4, the craters do not continue increasing in radial size as evaporation is slowed. Instead the final rim height is reduced, and the disturbance in the free surface does not extend beyond $8L$, even with the slowest evaporation rate.

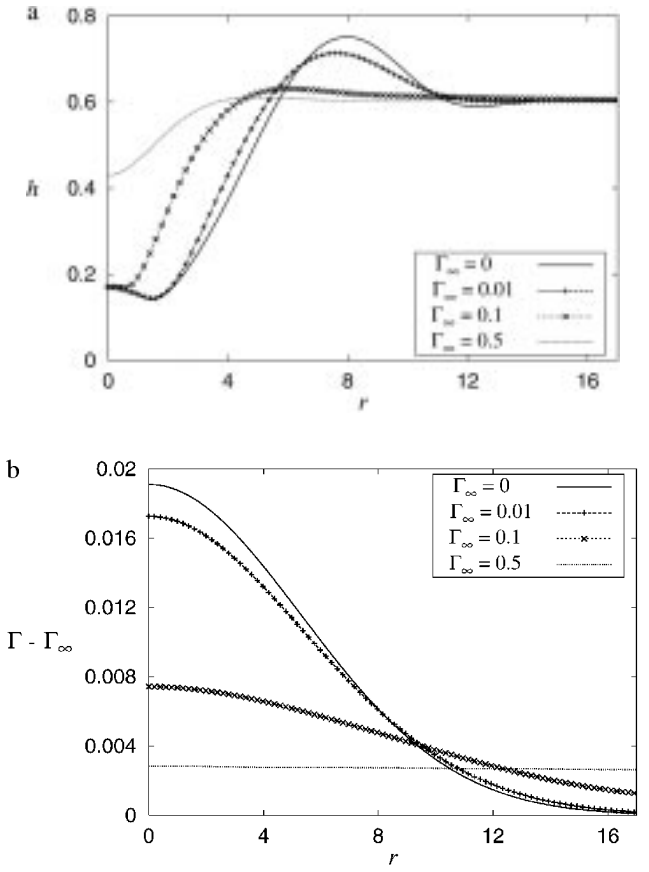

FIG. 13. Craters in the paint described in Table 1, when there is a uniform preexisting surfactant layer, with initial concentration Γ_∞ varying between 0 (no preexisting surfactant) and 0.5, on an initially flat paint layer. A bolus of surfactant with concentration $\Gamma_0 = 1$ is added, causing a crater to form: (a) final coating profile h, (b) final excess surfactant distribution $\Gamma - \Gamma_\infty$. All other parameters are the same as in Fig. 2. An initial surfactant layer prevents formation of a severe crater.

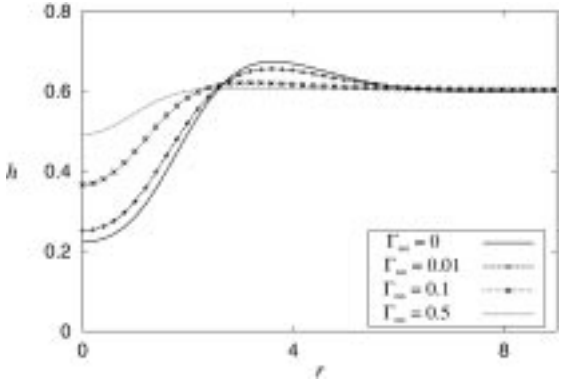

FIG. 14. Craters in the paint described in Table 1, showing the final coating profile h, when there is uniform preexisting surfactant, with initial concentration Γ_∞ varying between 0 (no preexisting surfactant) and 0.5. The paint layer is initially flat. A surfactant source, described by [24], with strength $Q_s = 0.01$ releases surfactant, causing the crater. Other parameters are the same as in Fig. 9. As for the bolus-driven crater, an initial surfactant layer significantly reduces the size of the final crater.

Furthermore the central peak, visible at all the evaporation rates shown in Fig. 4, disappears at the lower evaporation rates when $\Gamma_\infty = 0.1$, due to enhanced back-flow.

A mathematical explanation for the calming effect of preexisting surfactant is that it results from the nonlinearity of the surfactant evolution equation, even when surface tension depends linearly on concentration. Without leveling and evaporation, Eq. [19] becomes

$$\frac{\partial \Gamma}{\partial t} + \nabla \cdot \left(\frac{h}{\mu} \frac{d\sigma}{d\Gamma} \Gamma \nabla \Gamma \right) = 0.$$

Transport of surfactant is therefore enhanced in regions where there is already a high surfactant concentration.

4.4. A Simplified Model for Drying

The results presented above suggest that the effect of the drying model on the evolution of the crater is approximately that of setting a "stopping time" for spreading. An adequate approximation to the solution of the full problem, which includes resin transport and viscosification, may be obtained by simulating a constant viscosity, nonevaporating layer, halting at an appropriate time. The coating layer thickness is then adjusted to reflect solvent removal by evaporation.

The thickness $h(t)$ of a uniform layer of paint evaporating at constant evaporation rate e_0 is

$$h(t) = H - e_0 t$$

or in dimensionless form, using the definitions of Section 3,

$$h^*(t^*) = 1 - E t^*.$$

Thus for a uniform layer the resin concentration

$$c(t) = \frac{h_r}{h(t)} = \frac{c_0}{1 - E t^*}$$

and the viscosity $\mu(t) = \mu(c(t))$ are known functions of time. The final layer thickness is merely $h_r = c_0 H$.

If it is assumed that during cratering the resin concentration and paint viscosity do not vary appreciably along the substrate, then viscosity may be taken outside the spatial gradient operators in [17] and [19]. While Figs. 2 and 9 show that this is certainly not always the case, the method here will be seen to be successful nevertheless. Following Overdiep (35), a new "effective" time variable or fluidity Φ is defined by

$$\frac{d\Phi}{dt} = \frac{\mu_0}{\mu(t)},$$

which accounts for retardation of the flow due to viscosity increase. Integrating until the paint is dry at T_d gives the effective

dimensionless stopping time

$$\Phi_{\mathrm{d}} = \int_0^{T_{\mathrm{d}}} \frac{\mu_0}{\mu(\tilde{t})}\, d\tilde{t} \qquad [26]$$

required for a run with no viscosification or evaporation. Replacing t by Φ in the evolution equations for h and Γ, neglecting surfactant diffusion, yields

$$\frac{\partial h}{\partial \Phi} = -\nabla \cdot (h^3 \nabla \nabla^2 h + A h^2 \nabla \sigma), \qquad [27]$$

$$\frac{\partial \Gamma}{\partial \Phi} = -\nabla \cdot \left(\left[\frac{3}{2} h^2 \nabla \nabla^2 h + 2Ah \nabla \sigma \right] \Gamma \right) + \frac{\mu(t)}{\mu_0} Q_\Gamma. \qquad [28]$$

The viscosity now only appears in a time-dependent surfactant source term, which requires knowledge of μ as a function of Φ. For simplicity, this method is only applied to bolus-driven craters here.

For the parameters used in Section 4.1 ($E = 0.0048$, $c_0 = 0.6$, $M = 25$, $B = 4$), drying a uniform paint would take until $t = T_{\mathrm{d}} = 83.33T$, while computing the integral in [26] numerically gives $\Phi_{\mathrm{d}} = 3.266$. The severe increase in viscosity as solvent is removed requires that a simulation with constant viscosity be halted considerably earlier than the "viscosifying" solution. Such a simulation is shown in Fig. 15, which shows the coating profile at $\Phi = 3.266$ obtained by a model run without evaporation or viscosification and the same profile rescaled by c_0 to simulate solvent removal, compared against the result of a simulation with both evaporation and viscosification, which stops at $t = 102.6T$. The method produces a generally similar dry crater but slightly overestimates amplitude of the coating disturbance. This is to be expected because shrinkage of the coating during drying increases its resistance to the flow.

The general features of the crater, as produced by the simple and full models, are similar. This indicates that these features are robust, i.e., do not depend on the particular drying model used.

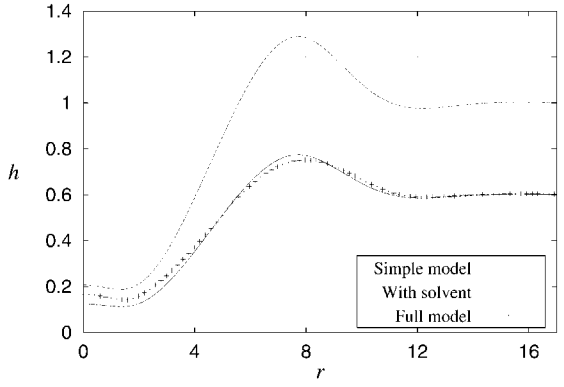

FIG. 15. Comparison of the full model to a simpler one excluding viscosification and evaporation. Broken line indicates the solution $h(r, t)$ obtained by the model without viscosification or evaporation at $t = 3.266$; solid line indicates $c_0 h(r, t)$, corresponding to removal of all solvent. Points (+) show the final dry profile obtained using the evaporating, viscosifying model. ($E = 0.0048$, $c_0 = 0.6$, $M = 25$, $B = 4$.)

5. DISCUSSION AND SUMMARY

We have developed a mathematical model of the cratering of a paint during drying in the presence of a surfactant. The model paint is an idealization of a real paint containing many interacting components, which consists of just two parts, a volatile and a nonvolatile component. As the volatile component is removed by evaporation, the paint viscosity increases until further flow is prevented. Nonuniform surfactant on the free surface of the film generates surface tension gradients, and the resulting shear stresses drive the outward flow which is responsible for crater formation. Because paint films are thin, lubrication theory is used to reduce the governing equations to three coupled partial differential equations. For craters which develop in an axisymmetric manner, a finite difference method involving only one space dimension was implemented to solve the model equations. Gravitational effects have been neglected here, though their inclusion would be straightforward. The model was used to show the craters formed by two different processes.

In the first mechanism, which might be appropriate for surfactant falling on the film from above, a large concentration of surfactant is initially released in a small region of the film. This creates strong initial surface tension gradients which quickly carry paint and surfactant outward. The precise shape of the initial surfactant distribution is only important in determining the shape of the inner part of the resulting crater. A smooth initial distribution produces a crater with a smooth center, while with a less smooth distribution, the model leads to the commonly observed central peak seen by Weh and Linde (3) and others. While the shape of the surfactant distribution has a minor effect on most of the crater, the total amount of surfactant in the bolus M_Γ strongly affects the crater radius and depth. Surfactant diffusion, both along the paint surface and from the surface into the paint layer, reduces the depth of cratering and the slopes of the crater walls.

For a range of evaporation rates, it was found that increasing the evaporation parameter E leads to broader craters. The final coating profiles obtained for bolus-driven craters form a single self-similar family, in the sense that when the radial coordinate r is replaced by the scaled variable $\xi = r/t_{\mathrm{dry}}^{1/4}$ (where t_{dry} is the time at which drying is complete for each value of E), the outer part of the crater is described by a single function of ξ. This scaling has been identified (16, 12) as appropriate for spreading of an insoluble surfactant by flow driven only by surface tension gradients and opposed by viscosity. That it continues to work when paint-drying features, viscosification and solvent evaporation, are present suggests that these features can be considered independent of STG flow as an initial approximation. Near $\xi = 0$ there are necessarily differences, as the boundary conditions for the similarity solution are zero film thickness and infinite

surfactant concentration there. Self-similar collapse does not occur when there is preexisting surfactant.

For bolus-driven craters we demonstrated that a simulation of surfactant spreading on a constant viscosity, nonevaporating coating can be used to approximate the results of the model including drying and viscosification, with reasonable success. This demonstrates the robustness of the model: the general features of the crater are unaltered by this change to the drying model. This simpler method is potentially useful in industrial application of the model.

The second mechanism used is a fixed source supplying surfactant to a region of the paint at a steady rate, which may represent the gradual release of surfactant from a large particle contacting the surface. By this means, the model forms deep craters, removing essentially all the paint near the source, nearly down to the substrate. Increasing the total amount of surfactant available to drive the flow, whether by faster release or slower evaporation, leads to larger craters. This can result in a relatively flat central region, thinnest just inside the steepest part of the crater rim, where rupture may take place, as described by Kheshgi and Scriven (34). Increasing surfactant diffusivity or incorporating bulk diffusion of surfactant into the film tends to reduce both the rim height and depth of craters. A constant surfactant supply rate has been used, though it seems likely that in reality a source will reduce in strength, with the surfactant supply rate, $q_\Gamma(r, t)$ decreasing over time.

Certain features are common to both cratering mechanisms. Both produce craters of considerably larger diameter than the source of surfactant causing them, as has been observed experimentally (see, e.g., (5)). The inner part of the crater dries first, because the coating layer is thinner there, so a greater fraction of the solvent is removed by evaporation in a given time. A reduction in the rate of increase of viscosity during drying leads to large craters because higher flow rates are possible. Preexisting levels of surfactant can substantially reduce the severity (both size and depth) of defects in the dried coating for both of the cratering mechanisms considered above.

One might expect that drying the paint at a slower rate would allow more time for leveling, resulting in a less pronounced defect. However, reducing the drying parameter E produces craters which are both larger and deeper. These results suggest that the drying should be rapid, or the paint very viscous, in order to limit crater development. This situation arises because leveling is relatively ineffective in eliminating craters, in our simulations. There is a disparity in the time scales associated with STG effects and leveling. The time scale for the former is

$$T_{\mathrm{stg}} = \frac{2\mu_0}{\sigma_0 - \sigma_\infty}\frac{L^2}{H^2} = \frac{T}{A},$$

while the latter scales with T. Since $A \gg 1$, the initial growth of the crater occurs before leveling effects become significant. The time scale for evaporation to dry the film is $T_{\mathrm{d}}T$, with $T_{\mathrm{d}} \gg 1$ in general. However, the viscosity increase in the paint effectively increases both T_{stg} and T as drying continues, until no further flow is possible. There is therefore little opportunity for leveling to reduce the severity of cratering. If the drying rate were to reduce as drying progresses, as is known to occur (36), the required drying time would increase, potentially aiding leveling.

Our results agree qualitatively with general descriptions of craters regarding their size and structure (a pronounced rim, sometimes a central peak, rapid formation). More detailed validation would be the subject of future research. Our model may be used as a tool to provide insight into industrial cratering problems. However, it still requires more realistic functional forms for the drying rate, surface tension, and viscosity. This would allow investigators to better understand the craters which arise in actual coatings, and to evaluate possible measures for their prevention or control, before beginning production. Additional factors, such as skin formation and top-down drying, may also require inclusion. Coatings developers may be able to deduce something of the properties of agents causing a crater from a study of its size, depth, or growth time. A few simulations could then reduce the need for extensive, expensive, testing of coating samples.

ACKNOWLEDGMENTS

This work is supported by the ICI Business Link Partnership, the NASA Microgravity Program, and the State of Delaware.

REFERENCES

1. Kornum, L. O., and Raaschou Nielsen, H. K., *Prog. Org. Coat.* **8,** 275 (1980).
2. Pierce, P. E., and Schoff, C. K., "Coating Film Defects," Federation Series on Coatings Technology. Federation of Societies for Coatings Technology, Philadelphia, PA, 1988.
3. Weh, L., and Linde, H., *Plaste Kautsch.* **20,** 849 (1973).
4. Hahn, F. J., *J. Paint Technol.* **43,** 58 (1971).
5. Hahn, F. J., and Steinhauer, S., *J. Paint Technol.* **47,** 54 (1975).
6. Bierwagen, G. P., *Prog. Org. Coat.* **3,** 101 (1975).
7. Ahmad, J., and Hansen, R. S., *J. Colloid Interface Sci.* **38,** 601 (1972).
8. Gaver, D. P., and Grotberg, J. B., *J. Fluid Mech.* **235,** 399 (1992).
9. Grotberg, J. B., and Gaver, D. P., *J. Colloid Interface Sci.* **178,** 377 (1996).
10. Borgas, M. S., and Grotberg, J. B., *J. Fluid Mech.* **193,** 151 (1988).
11. Gaver, D. P., and Grotberg, J. B., *J. Fluid Mech.* **213,** 127 (1990).
12. Jensen, O. E., and Grotberg, J. B., *J. Fluid Mech.* **240,** 259 (1992).
13. Jensen, O. E., and Grotberg, J. B., *Phys. Fluids A* **5,** 58 (1993).
14. Fraaije, J. G. E. M., and Cazabat, A. M., *J. Colloid Interface Sci.* **133,** 452 (1989).
15. Ramos de Souza, E., and Gallez, D., *Phys. Fluids* **10,** 1804 (1998).
16. Espinosa, F. F., Master's thesis, Massachusetts Institute of Technology, 1991.
17. Espinosa, F. F., Shapiro, A. H., Fredberg, J. J., and Kamm, R. D., *J. Appl. Physiol.* **75,** 2028 (1993).
18. Shen, H., and Hartland, S., *J. Colloid Interface Sci.* **167,** 94 (1994).
19. Schwartz, L. W., Weidner, D. E., and Eley, R. R., *Langmuir* **11,** 3690 (1995).
20. Schwartz, L. W., Cairncross, R. A., and Weidner, D. E., *Phys. Fluids* **8,** 1693 (1996).
21. Stratta, J. J., Dillon, P. W., and Semp, R. H., *J. Coat. Technol.* **50,** 39 (1978).
22. Weidner, D. E., Schwartz, L. W., and Eley, R. R., *J. Colloid Interface Sci.* **179,** 66 (1996).
23. Howison, S. D., Moriarty, J. A., Ockendon, J. R., Terrill, E. L., and Wilson, S. K., *J. Engineering Math.* **32,** 377 (1997).

24. Eres, M. H., Weidner, D. E., and Schwartz, L. W., *Langmuir* **15,** 1859 (1999).
25. Heiple, C. R., and Roper, J. R., *Weld. Res. (Miami)* (1982).
26. Zacharia, T., and David, S. A., *in* "Mathematical Modelling of Weld Phenomena." Inst. of Materials, 1993.
27. Bäuerle, D., "Laser Processing and Chemistry," 2nd ed. Springer-Verlag, Berlin, 1996.
28. Fanton, X., and Cazabat, A. M., *Langmuir* **14,** 2554 (1998).
29. Bikerman, J. J., "Surface Chemistry: Theory and Applications," 2nd ed. Academic Press, New York, 1958.
30. Sheludko, A., *Adv. Colloid Interface Sci.* **1,** 391 (1967).
31. Orchard, S. E., *Appl. Sci. Res., Sect. A* **11,** 451 (1962).
32. Peaceman, D. W., and Rachford, H. H., *J. Soc. Indust. Appl. Math.* **3,** 28 (1955).
33. Ruckenstein, E., and Jain, R. K., *J. Chem. Soc., Faraday Trans. 2* **70,** 132 (1974).
34. Kheshgi, H. S., and Scriven, L. E., *Chem. Eng. Sci.* **46,** 519 (1991).
35. Overdiep, W. S., *Prog. Org. Coat.* **14,** 159 (1986).
36. Hansen, C. M., *Ind. Eng. Chem. Prod. Res. Dev.* **9,** 282 (1970).